ISSN 1674-1056
http://cpb.iphy.ac.cn
http://iopscience.iop.org/cpb
中国物理 B
Chinese Physics
中国物理 Chinese Physics B

Structural and electrical transport properties of Dirac-like semimetal $PdSn_4$ under high pressure

Bowen Zhang(张博文)[1,2], Chao An(安超)[3,4], Yonghui Zhou(周永惠)[1], Xuliang Chen(陈绪亮)[1], Ying Zhou(周颖)[3], Chunhua Chen(陈春华)[1,2], Yifang Yuan(袁亦方)[1,2], Zhaorong Yang(杨昭荣)[1,3,5]

Citation: Chin. Phys. B . 2019, 28(12): 126202 . **doi:** 10.1088/1674-1056/ab50b3
Journal homepage: http://cpb.iphy.ac.cn; http://iopscience.iop.org/cpb

What follows is a list of articles you may be interested in

High-pressure electrides: From design to synthesis

Biao Wan(万彪), Jingwu Zhang(张静武), Lailei Wu(吴来磊), Huiyang Gou(缑慧阳)

Chin. Phys. B . 2019, 28(10): 106201 . **doi:** 10.1088/1674-1056/ab3f95

Phase transitions in bismuth under rapid compression

Dong-Liang Yang(杨栋亮), Jing Liu(刘景), Chuan-Long Lin(林传龙), Qiu-Min Jing(敬秋民), Yi Zhang(张毅), Yu Gong(宫宇), Yan-Chun Li(李延春), Xiao-Dong Li(李晓东)

Chin. Phys. B . 2019, 28(3): 036201 . **doi:** 10.1088/1674-1056/28/3/036201

Pressure-induced enhancement of optoelectronic properties in PtS_2

Yi-Fang Yuan(袁亦方), Zhi-Tao Zhang(张志涛), Wei-Ke Wang(王伟科), Yong-Hui Zhou(周永惠), Xu-Liang Chen(陈绪亮), Chao An(安超), Ran-Ran Zhang(张冉冉), Ying Zhou(周颖), Chuan-Chuan Gu(顾川川), Liang Li(李亮), Xin-Jian Li(李新建), Zhao-Rong Yang(杨昭荣)

Chin. Phys. B . 2018, 27(6): 066201 . **doi:** 10.1088/1674-1056/27/6/066201

Neutron powder diffraction and high-pressure synchrotron x-ray diffraction study of tantalum nitrides

Lei-hao Feng(冯雷豪), Qi-wei Hu(胡启威), Li Lei(雷力), Lei-ming Fang(房雷鸣), Lei Qi(戚磊), Lei-lei Zhang(张雷雷), Mei-fang Pu(蒲梅芳), Zi-li Kou(寇自力), Fang Peng(彭放), Xi-ping Chen(陈喜平), Yuan-hua Xia(夏元华), Yohei Kojima(小岛洋平), Hiroaki Ohfuji(大藤宏明), Duan-wei He(贺端威), Bo Chen(陈波), Tetsuo Irifune(入舩徹男)

Chin. Phys. B . 2018, 27(2): 026201 . **doi:** 10.1088/1674-1056/27/2/026201

Exploring the compression behavior of HP-$BiNbO_4$ under high pressure

Yin-Juan Liu(刘银娟), Jia-Wei Zhang(张佳威), Duan-Wei He(贺端威), Chao Xu(许超), Qi-Wei Hu(胡启威), Lei Qi(戚磊), A-Kun Liang(梁阿坤)

Chin. Phys. B . 2017, 26(11): 116202 . **doi:** 10.1088/1674-1056/26/11/116202

Structural and electrical transport properties of Dirac-like semimetal $PdSn_4$ under high pressure*

Bowen Zhang(张博文)[1,2], Chao An(安超)[3,4,†], Yonghui Zhou(周永惠)[1], Xuliang Chen(陈绪亮)[1], Ying Zhou(周颖)[3], Chunhua Chen(陈春华)[1,2], Yifang Yuan(袁亦方)[1,2], and Zhaorong Yang(杨昭荣)[1,3,5,‡]

[1] *Anhui Province Key Laboratory of Condensed Matter Physics at Extreme Conditions, High Magnetic Field Laboratory, Chinese Academy of Sciences, Hefei* 230031, *China*

[2] *University of Science and Technology of China, Hefei* 230026, *China*

[3] *Institutes of Physical Science and Information Technology, Anhui University, Hefei* 230601, *China*

[4] *Key Laboratory of Structure and Functional Regulation of Hybrid Materials (Anhui University), Ministry of Education, Hefei* 230601, *China*

[5] *Collaborative Innovation Center of Advanced Microstructures, Nanjing* 210093, *China*

(Received 16 September 2019; revised manuscript received 21 October 2019; published online 22 November 2019)

We conducted *in-situ* high-pressure synchrotron x-ray diffraction (XRD) and electrical transport measurements on Dirac-like semimetal $PdSn_4$ in diamond anvil cells with quasi-hydrostatic pressure condition up to 44.5 GPa–52.0 GPa. The XRD data show that the ambient orthorhombic phase (*Ccca*) is stable with pressures to 44.5 GPa, and the lattice parameters and unit-cell volume decrease monotonously upon compression. The temperature dependence of the resistance exhibits a metallic conduction and follows a Fermi-liquid behavior below 50 K, both of which keep unchanged upon compression to 52.0 GPa. The magnetoresistance curve at 5 K maintains a linear feature in a magnetic field range of 2.5 T–7 T with increasing pressure to 20.0 GPa. Our results may provide pressure-transport constraints on the robustness of the Dirac fermions.

Keywords: high pressure, Dirac-like semimetal, crystal structure, electrical transport

PACS: 62.50.–p, 61.05.C–, 72.15.–v, 74.62.Fj **DOI:** 10.1088/1674-1056/ab50b3

1. Introduction

Topological semimetals (TSMs) draw a great deal of attention in recent years due to their unique topological properties and potential applications in spintronics.[1–9] In general, TSMs host points or lines in the momentum space where the conduction and the valence bands of TSMs cross linearly, leading to exotic properties, such as high mobility, chiral anomaly, and extremely large magnetoresistance (XMR). Two prominent examples of topological semimetals with zero-dimensional (0D) band crossing points are the Dirac and Weyl semimetals, such as Na_3Bi,[1] Cd_3As_2,[2,3] PtX_2 (X = Se, Te),[4,5] TaAs family,[6–8] and WTe_2.[9] When conduction and valence bands cross to form a one-dimensional (1D) closed loop in momentum space, another type of semimetal named nodal-line topological semimetal is formed, like $PbTaSe_2$[10] and ZrSiS.[11,12] Recently, a novel Dirac node arc topological structure was reported in ultrahigh magnetoresistive material $PtSn_4$.[13] Unlike the closed loops of line nodes, the Dirac node arc structure arises owing to the surface states and the Dirac dispersion is extended along a short line in the momentum space.[13]

As a homologue of the Dirac nodal arc semimetal $PtSn_4$,[13] Dirac-like features were recently discovered in $PdSn_4$ through angle-resolved photoemission spectroscopy (ARPES) experiments, which is in consistence with band-structure calculations.[14] At ambient pressure, $PdSn_4$ shows a metallic behavior in the temperature range of 1.8 K–300 K and follows Fermi-liquid behavior at low temperatures. The XMR of $PdSn_4$ reaches 7.5×10^4% at 1.8 K and 14 T, with external magnetic field perpendicular to b axis.[14] Based on detailed analysis of the magnetoresistance experiments, both carrier compensation and emergence of an excitonic insulating state were ruled out as the main origins of the XMR in $PdSn_4$.[14]

As one of the fundamental state parameters, high pressure is a clean and effective tool to tune lattice as well as electronic states, especially in topological quantum materials.[15,16] For example, in the case of type-II Weyl semimetal WTe_2, superconductivity was observed by application of high pressure.[15–17] To date, the high-pressure electronic properties of $PdSn_4$ was investigated only up to 2.5 GPa,[18] in which the author believed that the variation of

*Project supported by the National Key Research and Development Program of China (Grant Nos. 2018YFA0305700 and 2016YFA0401804), the National Natural Science Foundation of China (Grant Nos. U1632275, 11574323, 11874362, 11704387, and 11804344), the Natural Science Foundation of Anhui Province, China (Grant Nos. 1908085QA18, 1708085 QA19, and 1808085MA06), the Major Program of Development Foundation of Hefei Center for Physical Science and Technology, China (Grant No. 2018ZYFX002), and the Users with Excellence Project of Hefei Science Center of the Chinese Academy of Sciences (Grant No. 2018HSC-UE012).

†Corresponding author. E-mail: chaoan@ahu.edu.cn

‡Corresponding author. E-mail: zryang@issp.ac.cn

© 2019 Chinese Physical Society and IOP Publishing Ltd

the resistivity under pressure might be related to a change of Fermi surface topography.[18]

To further investigate the pressure effect on electronic properties of $PdSn_4$ at higher pressure and its relationship with lattice structure, we carried out high-pressure powder x-ray diffraction and electrical transport measurements on $PdSn_4$ single crystals. We show that there is no structural transition upon compression up to 44.5 GPa. With increasing pressure, the temperature-dependent resistance maintains a metallic behavior till 52.0 GPa, with the magnetoresistance mechanism remaining unchanged at least up to 20 GPa.

2. Experimental details

Single crystals of $PdSn_4$ were synthesized by Sn self-flux method.[14] Excessive Sn trapped on the crystal surface was removed by centrifuging. The high quality of the single crystal was checked by x-ray diffraction (XRD) and energy-dispersive x-ray spectra (EDS) (see in Fig. 1). Magnetization measurements were conducted using a superconducting quantum interference device magnetometer. The high-pressure electrical transport measurements were performed in a Be–Cu diamond anvil cell (DAC) in a temperature range of 5 K–300 K by using standard four-probe method. The diameter of the diamond culet is 300 μm. Sodium chloride (NaCl) powder was used as the pressure transmitting medium (PTM). A small sample (∼ 80 μm × 50 μm × 5 μm) crushed from bulk $PdSn_4$ single crystal was loaded in the cell and the applied magnetic field is perpendicular to the electric current.

Pressure was generated by a Mao–Bell-type symmetric DAC for the synchrotron XRD measurements. High pressure synchrotron powder XRD was performed at room-temperature at the beamline of 16 BM-D ($\lambda = 0.4133$ Å), HPCAT[19] of the Advanced Photon Source, Argonne National Laboratory. Daphne 7373 oil was used as the PTM. The DIOPTAS[20] program was used for image integrations and the Le Bail method was employed to fit the XRD data with the RIETICA software.[21] Pressure calibration was determined by ruby fluorescence method in all the mentioned experiments.[22]

3. Results and discussion

$PdSn_4$ crystallizes in an orthorhombic structure with space group *Ccca* (No. 68).[14] The lattice is composed of stacks of Pd atoms sandwiched between two coplanar Sn layers along *b* axis, as displayed in Fig. 1(a). Figure 1(b) shows

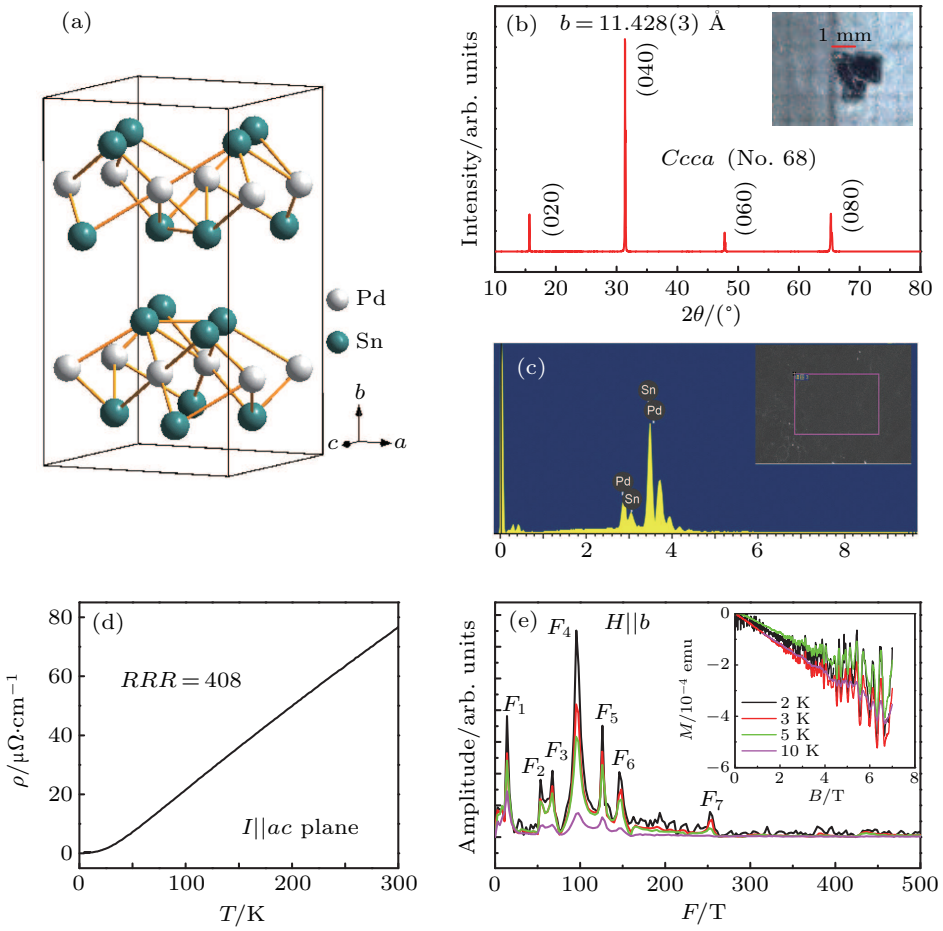


Fig. 1. (a) Crystal structure of $PdSn_4$, (b) XRD pattern of $PdSn_4$ single crystal. The reflection (0l0) is the as-grown crystal face. The upper-right inset shows an optical image of a $PdSn_4$ single crystal. Typical size of the sample is 2 mm× 2 mm× 1 mm. (c) Energy dispersive spectra of $PdSn_4$ single crystal. (d) Temperature-dependent resistivity of $PdSn_4$ single crystal with current along the *ac* plane. (e) Temperature dependence of the fast Fourier transformed dHvA data for $H \parallel b$. Inset shows the raw dHvA data.

a typical XRD pattern of $PdSn_4$ single crystal (λ = 1.54059 Å). The observation of only (010) reflections indicates a *b*-axis orientation of the as-grown crystals. The calculated lattice parameter *b* is 11.428(3) Å, in excellent accordance with previous report.[14] Energy dispersive x-ray spectra with area- and point-scanning modes give the ratio of Pd : Sn as 1 : 3.92(8) [Fig. 1(c)]. The temperature-dependent resistivity of $PdSn_4$ is displayed in Fig. 1(d). The residual resistivity ratio (*RRR*) of the sample is 408. In addition, magnetization of $PdSn_4$ was measured at different temperatures with external magnetic field along the *b* axis. Clear De Haas–Van Alphen oscillations (dHvA) are observed, as shown in the inset of Fig. 1(e). After using a fast Fourier transform (FFT) analysis, seven prominent frequencies labeled as F_1–F_7 are detected [Fig. 1(e)], in excellent accordance with that at ambient pressure.[14] These results indicate high quality of the as-grown $PdSn_4$ crystals.

We first investigated the evolution of the structure under high pressures. Figure 2 displays the selected XRD patterns of $PdSn_4$ at room temperature with pressures up to 44.5 GPa. At 0.5 GPa, the XRD peaks can be well indexed by the space group *Ccca* (No. 68), in accordance with that at ambient pressure.[14] We find that increasing pressure consistently pushes all Bragg peaks to higher angles, but no new peaks appear up to highest pressure studied. After the pressure is released down to ambient pressure, the peaks in the XRD pattern return to the initial positions [denoted by DP, at the top of Fig. 2(a)], which suggests the structural evolution is reversible.

To further analyze the XRD data, refinements were performed with Le Bail method by using the RIETICA software.[21] A typical XRD refinement result of 0.5 GPa is presented in Fig. 2(b), which gives $a = 6.410(7)$ Å, $b = 11.417(7)$ Å, and $c = 6.369(6)$ Å. The extracted lattice parameters (*a*, *b*, and *c*) are displayed in Fig. 2(d). With increasing pressure, all three lattice parameters decrease gradually. When the pressure increases up to 44.5 GPa, the fitting results in Fig. 2(c) show that the space group stays unchanged, while the lattice parameters are decreased by 8.4%–9.8%, *i.e.*, to $a = 5.871(0)$ Å, $b = 10.337(2)$ Å, and $c = 5.832(1)$ Å. In addition, pressure dependence of unit-cell volume (V) is fitted by using the third-order Birch–Murnaghan equation of state (EoS)[23] [red line in Fig. 2(e)]:

$$P = \frac{3}{2}B_0\left[(V_0/V)^{7/3} - (V_0/V)^{5/3}\right] \times \left\{1 + \frac{3}{4}(B_0' - 4)[(V_0/V)^{2/3} - 1]\right\}, \quad (1)$$

where V_0, B_0, and B_0' are the volume, bulk modulus $V/(\mathrm{d}V/\mathrm{d}P)$, and first-order derivative of the bulk modulus at zero pressure, respectively. The fitting yields $V_0 = 116.7$ (±2.4) Å^3, $B_0 = 89.0$ (±0.4) GPa, and $B_0' = 4.0$ (0). The refined lattice constants at various pressures are shown in Table 1.

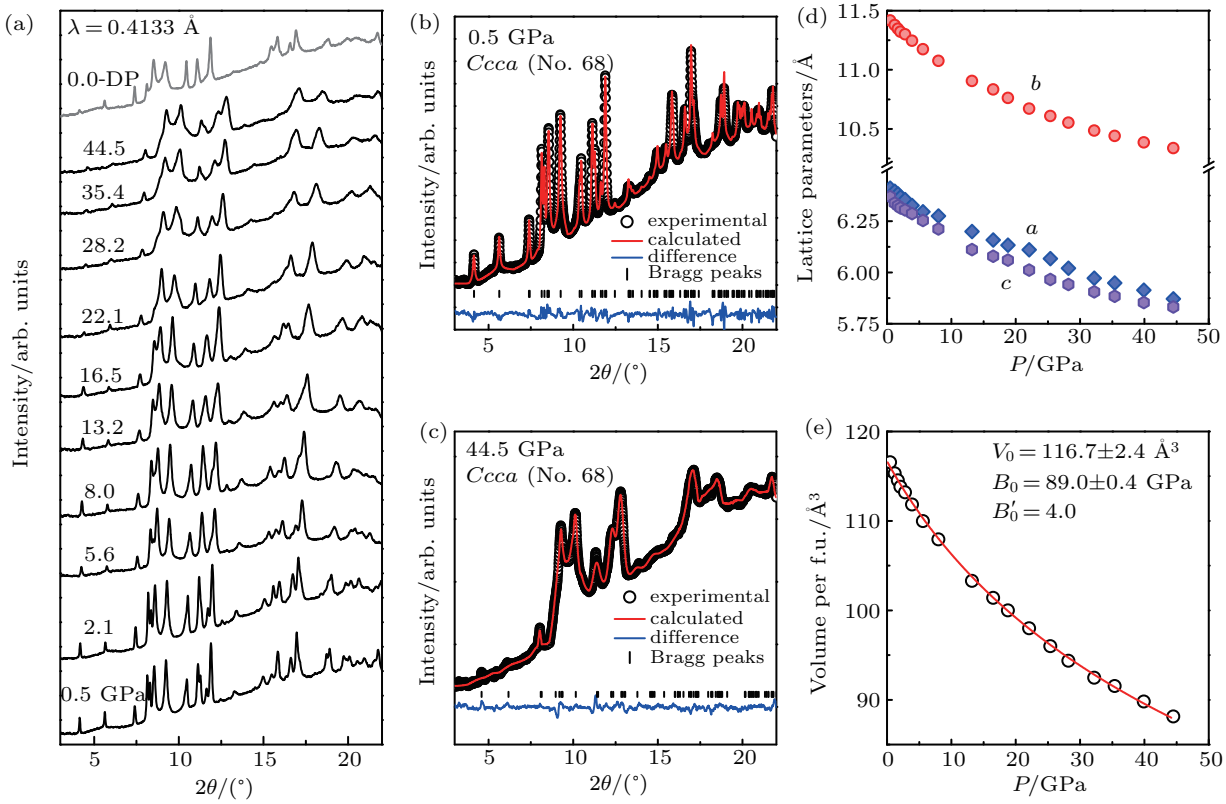


Fig. 2. (a) Synchrotron radiation x-ray diffraction patterns of $PdSn_4$ under pressures ($\lambda = 0.4133$ Å). The XRD pattern upon decompression back to 0.0 GPa is denoted by DP. (b) The refinements at (b) 0.5 GPa and (c) 44.5 GPa were performed by using the RIETICA program with the Le Bail method. (d) Pressure dependence of the refined lattice parameters. (c) The empty symbols stand for unit volume. The volume *versus* pressure data was fitted by the third-order Birch–Murnaghan formula (solid red line).

Table 1. Rietveld refined lattice constants of $PdSn_4$ at various pressures.

P/GPa	a/Å	b/Å	c/Å	R_p/%	R_{wp}/%
0.5	6.410(7)	11.417(7)	6.369(6)	2.2(8)	3.8(0)
1.2	6.395(8)	11.378(8)	6.337(9)	2.3(5)	3.9(2)
1.7	6.383(0)	11.346(7)	6.325(2)	3.1(5)	5.3(5)
2.1	6.367(6)	11.321(6)	6.315(1)	3.4(2)	6.0(8)
2.8	6.355(4)	11.300(0)	6.305(1)	2.3(5)	4.2(5)
3.9	6.326(6)	11.245(5)	6.287(3)	2.5(5)	3.8(1)
5.6	6.295(9)	11.173(7)	6.253(8)	2.1(8)	3.2(7)
8.0	6.275(2)	11.075(6)	6.212(5)	3.8(4)	7.2(0)
13.2	6.200(0)	10.905(2)	6.111(2)	2.4(5)	3.6(9)
16.5	6.158(5)	10.833(6)	6.078(8)	2.6(4)	4.2(0)
18.8	6.133(1)	10.761(3)	6.060(0)	2.0(4)	3.3(2)
22.1	6.110(7)	10.671(3)	6.011(4)	3.5(1)	5.9(2)
25.4	6.067(3)	10.609(2)	5.965(6)	2.4(1)	3.9(3)
28.2	6.020(4)	10.552(9)	5.941(1)	1.6(1)	2.3(7)
32.2	5.972(3)	10.485(9)	5.905(6)	2.6(8)	4.2(0)
35.4	5.949(0)	10.440(4)	5.884(4)	1.9(8)	3.1(3)
39.9	5.914(1)	10.385(7)	5.853(7)	1.9(0)	2.7(7)
44.5	5.871(0)	10.337(2)	5.832(1)	2.2(0)	3.2(7)

We further carried out high pressure transport measurements. Figure 3(a) shows the temperature (T) dependence of the electrical resistance (R) of single crystal $PdSn_4$ under various pressures. Starting at 3.2 GPa, $R(T)$ curve exhibits a metallic conductive behavior ($dR/dT > 0$) in the whole temperature range of 5 K–300 K, similar to that at ambient pressure.[14] Upon compression, metallic behaviors remain to the highest pressure of 52.0 GPa. Nevertheless, the resistance globally gets enhanced with increasing pressure. According to band theory, the pressure normally enhances the overlap of electronic orbitals and decrease the band gap, resulting in the decrement of resistance. However, we note that similar behavior of pressure-enhanced resistivity has also been observed in other TSMs, such as $TaSb_2$,[24] in which the reduction of carrier mobility under pressure is proposed due to the nonhydrostatic pressure condition, thus causing the enhancement in resistance. We find that the resistance (R) at high temperatures shows a quasi-linear temperature dependence behavior at various pressures, which suggest that the electron phonon scattering is the dominant scattering mechanism.[25] At temperatures below 50 K, the $R(T)$ curves at different pressures can be well described with the formula $R(T) = R_0 + AT^2$. Selected fitting of the $R(T)$ curves are displayed in Fig. 3(b), which suggest that the Fermi-liquid behavior remains unchanged under high pressure. As shown in Fig. 3(c), residual resistance R_0 monotonically increases upon compression without any anomaly.

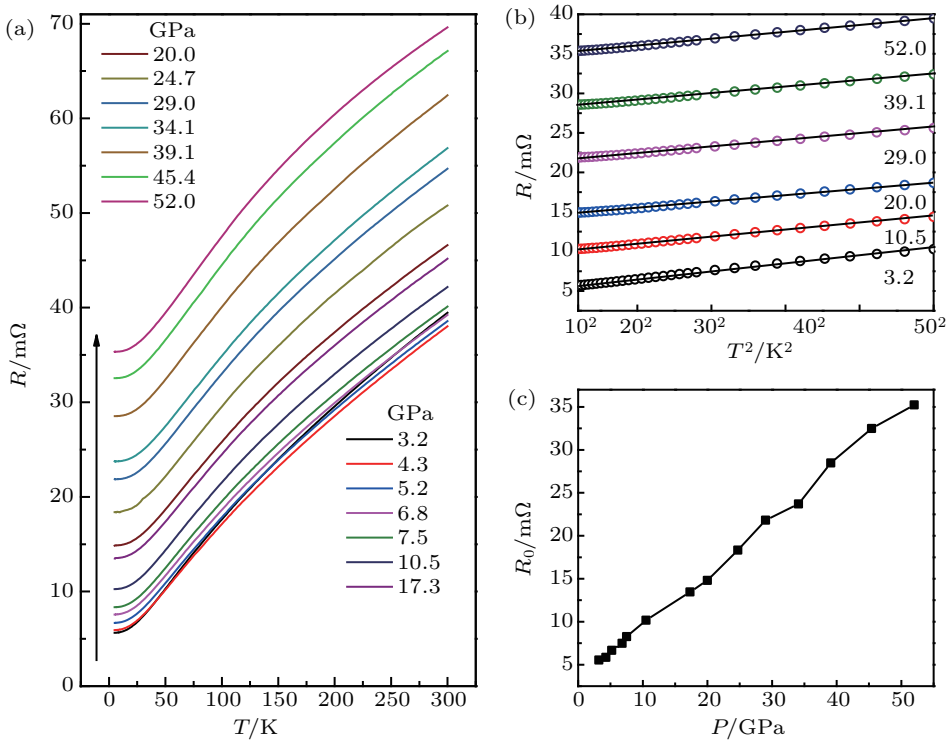


Fig. 3. (a) Temperature-dependent resistance of $PdSn_4$ in the pressure range of 3.2 GPa to 52.0 GPa from 5 K to 300 K. (b) Selected fitting results of R–T curves by using the power law. (c) The residual resistance R_0 as a function of pressure.

Since $PdSn_4$ possesses XMR effect, magnetoresistance $MR = [R(H) - R(0)]/R(0) \times 100\%$ measurements were performed at 5 K under various pressures. As shown in Fig. 4, one can see that the magnitude of MR (5 K, 7 T) is suppressed dramatically under high pressure. For example, it is 52.9% at 3.2 GPa and almost three orders smaller than that at ambient pressure.[14] Similar cases are also reported in TaAs[15] and WTe_2,[26] in which the suppressed MR under pressure is

attributed to reducing of the carrier mobility. In addition, we find that all *MR* curves can be divided into two parts. For example, at 3.2 GPa *MR* exhibits a conventional quadratic behavior below $\sim$ 2.5 T (red solid line), as shown in the inset of Fig. 4. By contrast, at high fields, *MR* gradually deviates from the quadratic relationship and develops into a linear field-dependent behavior (green dashed line), with no sign of saturation. The linear feature of *MR* at high fields or even at a full field range at a certain field orientation with respect to the *b* axis of single crystal $PdSn_4$ was also observed at ambient pressure, which is attributed to the existence of the Dirac-like linear dispersion.[18] In the quantum limit, all carriers are degenerate in the lowest Landau level. Thus once beyond a certain critical field B_c, quantum transport will dominate and a quadratic-to-linear *MR* transition will occur.[18] Similar behavior is also reported in charge density wave material $LaAgSb_2$.[27] With increasing pressure, *MR* decreases monotonously, however, the linear feature maintains up to 20 GPa, indicating the unchanged magnetoresistance mechanism. Considering the above experimental results and similar high-pressure studies on topological materials NbAs[28] and $TaSb_2$,[24] we infer that the robustness of the Dirac fermions of $PdSn_4$ possible be reflected under high pressure.

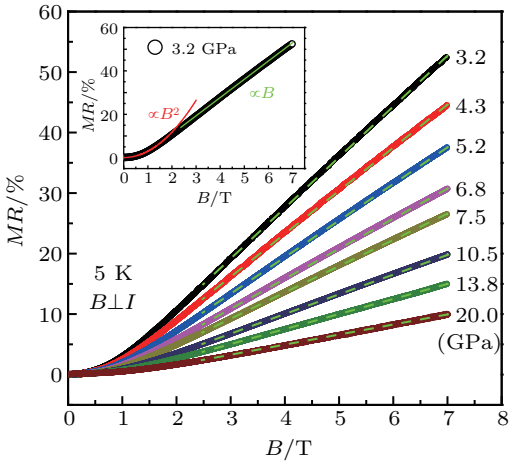


Fig. 4. Magnetoresistance *versus* applied field with $B \perp I$ under various pressures at 5 K. The inset shows a typical fitting of *MR* at 3.2 GPa. Red and green lines are fitting results at low and high magnetic field, respectively. The dashed green lines denote the linear behavior at various pressures.

4. Conclusions

In summary, we have investigated the pressure effect on the crystal structure and electronic properties of Dirac-like semimetal $PdSn_4$ single crystals. There are several main results: (i) *in situ* high-pressure synchrotron XRD data show that the crystal structure is stable up to 44.5 GPa with orthorhombic phase, (ii) *R*–*T* curves follow Fermi-liquid behavior below 50 K at various pressures, (iii) over the pressure range from 3.2 GPa to 20.0 GPa, the *MR* curves at 5 K maintain a linear field-dependent behavior above 2.5 T. Our study provides pressure-transport constraints on the robustness of the Dirac fermions of $PdSn_4$. Theoretical calculation on its topological states under pressure still need further investigation.

Acknowledgments

Portions of this work were performed at HPCAT (Sector 16), Advanced Photon Source (APS), Argonne National Laboratory. HPCAT operations are supported by DOE-NNSA's Office of Experimental Sciences. The Advanced Photon Source is a U.S. Department of Energy (DOE) Office of Science User Facility operated for the DOE Office of Science by Argonne National Laboratory under Contact No. DE-AC02-06CH11357.

References

[1] Liu Z K, Zhou B, Zhang Y, Wang Z J, Weng H M, Prabhakaran D, Mo S K, Shen Z X, Fang Z, Dai X, Hussain Z and Chen Y L 2014 *Science* **343** 864

[2] Liu Z K, Jiang J, Zhou B, Wang Z J, Zhang Y, Weng H M, Prabhakaran D, Mo S K, Peng H, DudinP, Kim T, Hoesch M, Fang Z, Dai X, Shen Z X, Feng D L, Hussain Z and Chen Y L 2014 *Nat. Mater.* **13** 677

[3] Borisenko S, Gibson Q, Evtushinsky D, Zabolotnyy V, Buchner B and Cava R J 2014 *Phys. Rev. Lett.* **113** 027603

[4] Li Y W, Xia Y Y Y, Ekahana S A, Kumar N, Jiang J, Yang L X, Chen C, Liu C X, Yan B H, Felser C, Li G, Liu Z K and Chen Y L 2017 *Phys. Rev. Mater.* **1** 074202

[5] Yan M, Huang H, Zhang K, Wang E, Yao W, Deng K, Wan G, Zhang H, Arita M, Yang H, Sun Z, Yao H, Wu Y, Fan S, Duan W and Zhou S 2017 *Nat. Commun.* **8** 257

[6] Huang X C, Zhao L X, Long Y J, Wang P P, Chen D, Yang Z H, Liang H, Xue M Q, Weng H M, Fang Z, Dai X and Chen G F 2015 *Phys. Rev. X* **5** 031023

[7] Lv B Q, Weng H M, Fu B B, Wang X P, Miao H, Ma J, Richard P, Huang X C, Zhao L X, Chen G F, Fang Z, Dai X, Qian T and Ding H 2015 *Phys. Rev. X* **5** 031013

[8] Xu N, Weng H M, Lv B Q, Matt C E, Park J, Bisti F, Strocov V N, Gawryluk D, Pomjakushina E, Conder K, Plumb N C, Radovic M, Autes G, Yazyev O V, Fang Z, Dai X, Qian T, Mesot J, Ding H and Shi M 2016 *Nat. Commun.* **7** 11006

[9] Wang C L, Zhang Y, Huan J W, Nie S M, Liu G D, Liang A J, Zhang Y X, Shen B, Liu J, Hu C, Ding Y, Liu D F, Hu Y, He S L, Zhao L, Yu L, Hu J, Wei J, Mao Z Q, Shi Y G, Jia X W, Zhang F F, Zhang S J, Yang F, Wang Z M, Peng Q J, Weng H M, Dai X, Fang Z, Xu Z Y, Chen C T and Zhou X J 2016 *Phys. Rev. B* **94** 241119(R)

[10] Bian G, Chang T R, Sankar R, Xu S Y, Zheng H, Neupert T, Chiu C K, Huang S M, Chang G, I B, Sanchez D S, Neupane M, Alidoust N, Liu C, Wang B K, Lee C C, Jeng H T, Zhang C L, Yuan Z J, Jia S, Bansil A, Chou F C, Lin H and Hasan M Z 2016 *Nat. Commun.* **7** 10556

[11] Schoop L M, Ali M N, Straßer C, Topp A, Varykhalov A, Marchenko D, Duppel V, Parkin S S P, Lotsch B V and Ast C R 2016 *Nat. Commun.* **7** 11696

[12] Neupane M, Belopolski I, Hosen M M, Sanchez D S, Sankar R, Szlawska M, Xu S Y, Dimitri K, Dhakal N, Maldonado P, Oppeneer P M, Kaczorowski D, Chou F C, Hasan M Z and Durakiewicz T 2016 *Phys. Rev. B* **93** 201104(R)

[13] Wu Y, Wang L L, Mun E, Johnson D D, Mou D X, Huang L N, Lee Y B, Bud'ko S L, Canfield P C and Kaminski A 2016 *Nat. Phys.* **12** 667

[14] Jo N H, Wu Y, Wang L L, Orth P P, Downing S S, Manni S, Mou D X, Johnson D D, Kaminski A, Bud'ko S L and Canfield P C 2017 *Phys. Rev. B* **96** 165145

[15] Pan X C, Chen X L, Liu H M, Feng Y Q, Wei Z X, Zhou Y H, Chi Z H, Pi L, Yen F, Song F Q, Wan X G, Yang Z R, Wang B G, Wang G H and Zhang Y H 2015 *Nat. Commun.* **6** 7805

[16] Zhou Y H, Lu P C, Du Y P, Zhu X D, Zhang G H, Zhang R R, Shao D X, Chen X L, Wang X F, Tian M L, Sun J, Wan X G, Yang Z R, Yang W G, Zhang Y H and Xing D Y 2016 *Phys. Rev. Lett.* **117** 146402

[17] Kang D, Zhou Y, Yi W, Yang C, Guo J, Shi Y, Zhang S, Wang Z, Zhang C, Jiang S, Li A, Yang K, Wu Q, Zhang G, Sun L and Zhao Z 2015 *Nat. Commun.* **6** 7804

[18] Xu C Q, Zhou W, Sankar R, Xing X Z, Shi Z X, Han Z D, Qian B, Wang J H, Zhu Z W, Zhang J L, Bangura A F, Hussey N E and Xu X F 2017 *Phys. Rev. Mater.* **1** 064201

[19] Park C, Popov D, Ikuta D, Lin C L, Kenney-Benson C, Rod E, Bommannavar A and Shen G Y 2015 *Rev. Sci. Instrum.* **86** 072205

[20] Prescher C and Prakapenka V B 2015 *High Press. Res.* **35** 223

[21] Hunter B A 1998 *Rietica — A Visual Rietveld Program*, International Union of Crystallography Commission on Powder Diffraction Newsletter No. 20 (Summer 1998), http://www.rietica.org

[22] Mao H K, Xu J and Bell P M 1986 *J. Geophys. Res.* **91** 4673

[23] Birch F 1947 *Phys. Rev.* **71** 809

[24] Zhou Y, Gu C C, Chen X L, Zhou Y H, An C and Yang Z Y 2018 *J. Solid State Chem.* **265** 359

[25] Zhang X, Xiao Z, Lei H, Toda Y, Matsuishi S, Kamiya T, Ueda S and Hosono H 2014 *Chem. Mater.* **26** 6638

[26] Cai P L, Hu J, He L P, Pan J, Hong X C, Zhang Z, Zhang J, Wei J, Mao Z Q and Li S Y 2015 *Phys. Rev. Lett.* **115** 057202

[27] Wang K F and Petrovic C 2012 *Phys. Rev. B* **86** 155213

[28] Zhang J, Liu F L, Dong J K, Xu Y, Li N N, Yang W G and Li S Y 2015 *Chin. Phys. Lett.* **32** 097102